A parametric study on the performance characteristics of an evacuated flat-plate photovoltaic/thermal (PV/T) collector

Mingke Hu [a], Chao Guo [b], Bin Zhao [c], Xianze Ao [c], Suhendri [a], Jingyu Cao [c], Qiliang Wang [d], Saffa Riffat [a], Yuehong Su [a, *], Gang Pei [c, *]

[a] *Department of Architecture and Built Environment, University of Nottingham, University Park, Nottingham NG7 2RD, UK*

[b] *Department of Severe Accident Analysis, China Nuclear Power Technology Research Institute, Shenzhen 518000, China*

[c] *Department of Thermal Science and Energy Engineering, University of Science and Technology of China, Hefei 230027, China*

[d] *Department of Building Services Engineering, The Hong Kong Polytechnic University, Kowloon, Hong Kong, China*

---

* Corresponding author: yuehong.su@nottingham.ac.uk; peigang@ustc.edu.cn

Abstract

An evacuated flat-plate photovoltaic/thermal (E-PV/T) collector was proposed. The inner space of the E-PV/T collector is vacuumed to suppress non-radiative heat losses, thus increasing thermal efficiency of the collector. Therefore, the E-PV/T collector has the potential to simultaneously deliver electricity and heat at high temperatures. A mathematic model was developed to evaluate the performance of the E-PV/T collector. The effect of some key parameters (e.g., initial water temperature in the water tank, vacuum degree, long-wave panel emissivity, and temperature coefficient of solar cells) on the performance of the E-PV/T system was investigated and the results were compared with a normal flat-plate PV/T (N-PV/T) system. Results suggest that the vacuum helps to enhance the total efficiency by nearly 10 percentage points in high-temperature conditions (＞80 °C). The vacuum degree of the upper space exerts a greater effect on system efficiencies compared to that of the lower space. Lower long-wave panel emissivity and greater temperature coefficient of the solar cell promote the performance of the collector. By lowering the long-wave panel emissivity from 0.95 to 0.05, the total efficiency soars from 26.82% to 61.20%. This study may help to guide parametric optimization and operation strategy of flat-plate PV/T collectors for high-temperature applications.

Keywords: *Solar energy; Evacuated flat-plate solar collector; Photovoltaic/thermal; PV/T; Parametric analysis.*

1. Introduction

Solar photovoltaic/thermal (PV/T) collectors can simultaneously provide electricity and heat by fully exploiting the solar radiation lies in the entire solar spectrum (0.2−3 μm), among which the flat-plate PV/T collector is the most common type due to its structural simplicity and building-integration easiness [1, 2]. Water and air, as two of the accessible natural working fluids, are widely employed in the PV/T system to cool the solar cells and collect thermal energy [3, 4]. Basically, the water-based PV/T collector shows better performance but faces the challenge of leakage and operating in freezing areas or seasons [5, 6]. By contrast, the air-based PV/T collector is free from leakage and freezing issues but may suffer from deteriorated electrical and thermal efficiencies [7]. Anyway, a PV/T collector is superior to the stand-alone solar PV panel and solar thermal collector in terms of overall performance [8].

However, as a part of solar energy is converted into electricity and the panel generally shows high long-wave emissivity, the flat-plate PV/T collector presents much lower thermal efficiency compared to the flat-plate solar thermal collector and thus is incapable of offering heat at relatively high temperatures [9]. A concentrated PV/T collector can work at high temperature but will bring unexpected side effect of adding the system complexity and cost [10, 11]. The normal flat-plate PV/T collector generally works in low-temperature conditions, indicating that the heated fluid it provided is mainly applied in domestic scenarios [12, 13], but is unable to effectively drive a thermodynamic system such as a solar-driven organic Rankine cycle (ORC) unit [14] or a solar-powered absorption chiller [15]. A higher temperature heat source is more valuable with a higher energy grade. Therefore, it will be would be beneficial and attractive to develop a flat-plate PV/T collector with high thermal efficiency and extend its application to fields requiring heat source with higher temperatures.

Reducing the heat loss of the PV/T collector working at high temperatures is a starting point to improve its thermal performance. As the absorber panel will be heated up to high temperatures when exposed to direct sunlight, the radiative heat loss of the panel will be increased dramatically therewith. Therefore, lowering the radiative heat loss of the PV/T panel is an effective strategy to elevate the thermal efficiency of a PV/T collector, especially when the panel temperature is at a high level. The normal PV/T collector shows high spectral absorptivity (emissivity) throughout the middle- and far-infrared wavelengths, indicating that a significant portion of absorbed heat is radiatively dissipated from the panel [16]. Therefore, inspired by the introduction of solar selective absorbing coatings in solar thermal collectors [17, 18], the thermal performance of a PV/T collector can be improved by cutting down the long-wave emissivity of the PV/T panel.

The conductive and convective heat losses of a PV/T collector also increase as the temperature of the panel and working fluid rise up, thus degrading the non-radiative heat loss is another route to improve the thermal efficiency of the flat-plate PV/T collector. Enlarging the thickness of the air gap and backside thermal insulation can suppress these heat losses but may also induce side effects of blocking a part of solar radiation and adding structural cumbersomeness [3, 19]. Considering that heat conduction and convection only take place with the help of a medium, the thermal performance of a PV/T collector will be enhanced if the PV/T panel is surrounded by a vacuum circumstance.

Creating a local vacuum environment for the absorber panel is actually a well-developed technology for solar thermal collection. The evacuated tube collector (ETC) has been introduced and developed for decades to collector hot water [20, 21]. The gap between two the concentric tubes is vacuumed, hence the non-radiative heat loss inside the ETC is deeply suppressed and the heat-collecting temperature is improved relative to the common flat-plate solar collector [22, 23]. Recently, the evacuated flat-plate collector has also been proposed and devised, in which the absorber panel is placed in a vacuum environment and is completely isolated to the glazing cover, backside thermal insulation, and side frames, therefore its conductive and convective heat losses are negligible and provide heat with relatively high temperature [24-30]. Farid et al. [26] fabricated two evacuated enclosures as prototype components for evacuated flat-plate solar collectors and tested the enclosures, respectively at 0.0033 Pa, 17 Pa, and atmospheric pressure, corresponding to stagnation temperature of 122.8, 104.2, and 103.6 °C for the absorber plate. Roger et al. [27] found that, after being evacuated to below 0.5 Pa, the heat loss coefficient of a solar collector dropped from 7.43 to 3.65 W/(m^2·K) and the efficiency under a nominal test condition increased from 36% to 56%. They also suggested that, by connecting the evacuated collector to an 85 °C district heating main, it would provide 66% more heat than the evacuated tube collectors and 112% more than the conventional flat plate collectors throughout a year. Gao et al. [31] conducted an experimental and numerical study on a flat-plate solar thermal collecting system which including 26 evacuated solar collectors with a total aperture area of 51 m^2. Results indicated that the thermal efficiency of the evacuated solar collector at zero-reduced temperature reached over 90%. In addition, the thermal and exergy efficiencies of the collector reached 59.67% and 14.35%, respectively when the inlet temperature, ambient temperature, and solar irradiation is correspondingly 123.0 °C, 35.7 °C, and 835.2 W/m^2.

Regarding the PV/T collector, only a few studies have involved introducing a vacuum scheme to improve the thermal efficiency of the collector. The idea of a vacuum encapsulated thin-film cell was introduced to suppress long-wave radiative heat loss by using the transparent electrode (TCO) of the thin-film cell, which shows high transmittance in the visible spectrum and high reflectance in the infrared band, as the upper surface [32]. Oyieke et al. [33] proposed a flat-plate vacuum insulated PV/T collector, in which the space between the glazing cover and PV module is filled with a vacuum insulation layer. Results revealed that the thermal and overall efficiencies of the vacuum insulated PV/T system increased by 9.5% and 16.8%, respectively, while the electrical efficiency reduced by 0.02% compared to the conventional PV/T system. Kutlu et al. [34] conceptually proposed a PV/T-ORC system combining amorphous silicon (a-Si) cells, evacuated flat plate solar collectors, and the ORC unit. Simulation results indicate that the a-Si PV/T-ORC system has the highest daily power output for a typical day, which is 102.3% more than the solar-powered ORC system, 23.8% more than the stand-alone poly-Si PV system and 12% more than the poly-Si PV/T-ORC system, respectively. Though these researches involve using vacuum mechanism to improve the thermal efficiency of the PV/T collector, a deeper and more thorough investigation focused on the performance of the evacuated PV/T collector, especially the evacuated flat-plate PV/T (E-PV/T), operating in different conditions is needed. The effect of some key structural and operational parameters on the electrical and thermal performance of the E-PV/T collector is lacked but can guide further optimization of the collector.

Under this context, a water-based evacuated flat-plate PV/T (E-PV/T) collector is proposed in the present study. A mathematic model is developed to evaluate the performance characteristics of the novel PV/T collector by comparing its efficiencies with a normal PV/T (N-PV/T) collector previously developed by the authors [35]. In addition, the effect of parameters such as the initial water temperature in the water tank, vacuum degree, long-wave (above 3 μm) panel emissivity, and temperature coefficient of solar cells on the performance of the E-PV/T system is numerically investigated.

2. Description of the evacuated PV/T collector

As shown in Fig. 1, the water-based E-PV/T collector, with an aperture area of 1.89 m^2, mainly consists of a glazing cover, a PV/T panel, backside thermal insulation, and frames. The glazing cover is 3.2 mm in thickness and shows a high transmittance in the solar spectrum. The PV/T panel is a key component of the collector, which including a PV layer, an aluminium substrate, a transparent Tedlar-Polyester-Tedlar (hereafter referred to as “TPT”) layer and a black TPT layer, seven copper water pipes, and two layers of EVA glue. The PV layer is made up of 72 mono-crystalline silicon solar cells, with a packing factor of 0.59, is laminated onto the aluminium substrate together with the black TPT layer. The transparent TPT layer is arranged on the surface of the panel and acts as an encapsulating layer of the PV modules. The seven copper pipes are connected with the back surface of the aluminium substrate. The backside thermal insulation material is a 30 mm-thick layer of glass fiber with thermal conductivity of 0.046 W/(m·K). The air gap between the glazing cover and absorber panel (hereafter referred to as the “upper space”) and the air interlayer between the absorber panel and backside thermal insulation (hereafter referred to as the “lower space”) are vacuumed to wipe out the non-radiative heat loss of the PV/T panel.

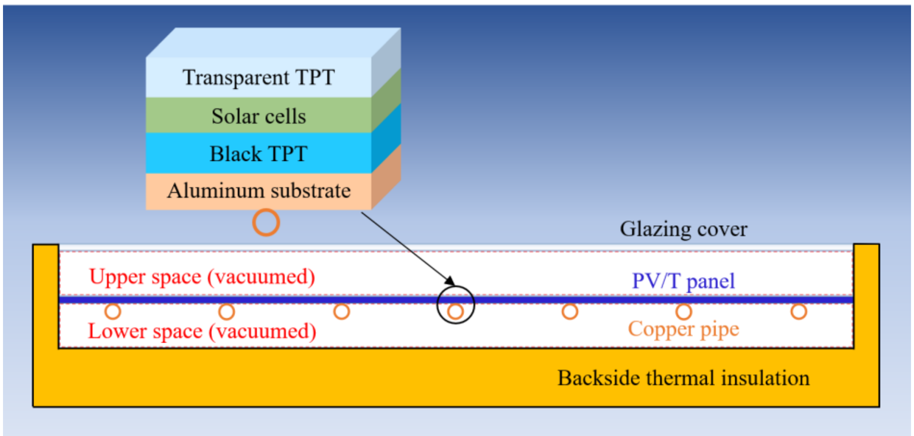

Fig. 1. The cross-section structure of the flat-plate E-PV/T collector.

Combining the E-PV/T collector with a 120 L circulating water tank, a water pump, and two connecting water pipes, an E-PV/T system is developed in this study. The schematic of the E-PV/T system is shown in Fig. 2.

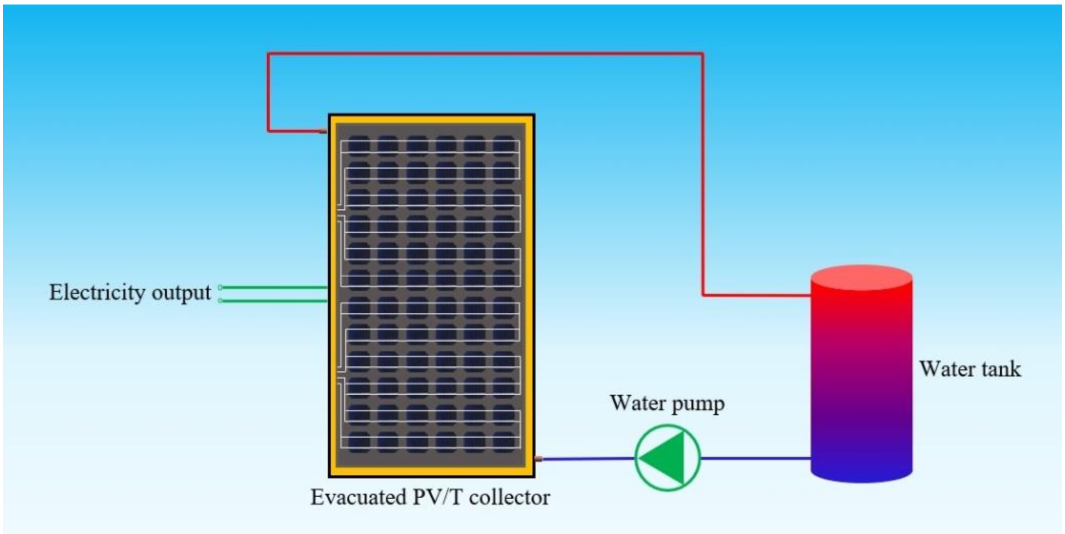

Fig. 2. The schematic of the flat-plate E-PV/T system.

3. Mathematic model

A mathematic model is developed to evaluate the performance of the E-PV/T system operating in dynamic-state conditions. According to the structure of the system, the mathematic model can mainly be divided into seven sub-models as follows:

- Sub-model for the glazing cover

- Sub-model for the PV layer
- Sub-model for the aluminium substrate
- Sub-model for the copper pipe
- Sub-model for the water in the copper pipe
- Sub-model for the backside thermal insulation
- Sub-model for the water tank

The schematic of the main energy exchanges within the flat-plate E-PV/T collector is shown in Fig. 3.

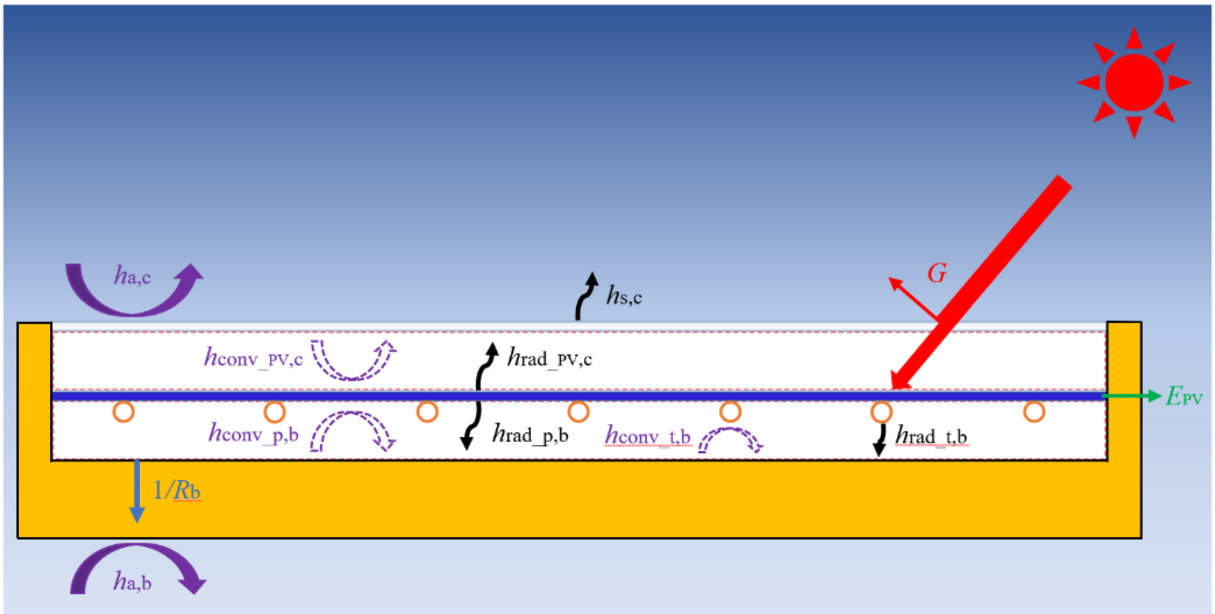

Fig. 3. The schematic of the main energy exchanges within the flat-plate E-PV/T collector. (The dashed arrows indicate that the value equals zero when the inner space is ideally vacuumed).

3.1 Glazing cover

The energy-balance equation of the glazing cover is expressed as:

$$\rho_c c_c d_c \frac{\partial T_c}{\partial t} = k_c d_c \frac{\partial^2 T_c}{\partial x^2} + h_{a,c}\left(T_a - T_c\right) + h_{s,c}\left(T_s - T_c\right) + h_{PV,c}\left(T_{PV} - T_c\right) + \alpha_{e\_c} G \tag{1}$$

where ρ_c and c_c refer to the density and specific heat capacity of the cover, kg/m^3 and J/(kg·K), respectively; T_c, T_a, T_s, and T_{PV} are the temperatures of the cover, ambient air, sky, and PV layer, respectively, K; t is the time step, s; x is the length direction of the PV/T collector, m; $h_{a,c}$ is the convective heat transfer coefficient between the cover and the ambient air, W/(m^2·K); $h_{s,c}$ is the radiative heat transfer coefficient between the cover and the sky, W/(m^2·K); $h_{PV,c}$ is the combined convective and radiative heat transfer coefficient between the cover and the PV layer, W/(m^2·K); α_{e_c} is the equivalent absorptivity of the cover; and G is the solar irradiance, W/m^2.

The convective heat transfer coefficient between the glazing cover and local outside surroundings is expressed as [9]:

$$h_{\mathrm{a,c}} = 2.8 + 3.0V_{\mathrm{a}} \tag{2}$$

where V_a is the ambient wind velocity, m/s.

The radiative heat transfer coefficient between the glazing cover and sky is written as [36]:

$$h_{\mathrm{s,c}} = \varepsilon_{\mathrm{c}}\sigma\left(T_{\mathrm{s}}^2 + T_{\mathrm{c}}^2\right)\left(T_{\mathrm{s}} + T_{\mathrm{c}}\right) \tag{3}$$

where ε_c refers to the emissivity of the glazing cover; σ is the Stefan–Boltzmann constant, 5.67×10^{-8} W/(m^2·K^4).

The combined convective and radiative heat transfer coefficient between the glazing cover and absorber panel is derived as [36]:

$$\begin{aligned} h_{\mathrm{PV,c}} &= h_{\mathrm{conv\_PV,c}} + h_{\mathrm{rad\_PV,c}} \\ &= \frac{Nu \cdot k_{\mathrm{a}}}{d_{\mathrm{gp}}} + \sigma\left(T_{\mathrm{PV}}^2 + T_{\mathrm{g}}^2\right)\left(T_{\mathrm{PV}} + T_{\mathrm{g}}\right)\left(\frac{\xi}{1/\varepsilon_{\mathrm{PV}} + \xi\left(1/\varepsilon_{\mathrm{g}} - 1\right)} + \frac{1-\xi}{1/\varepsilon_{\mathrm{TPT}} + \left(1-\xi\right)\left(1/\varepsilon_{\mathrm{g}} - 1\right)}\right) \end{aligned} \tag{4}$$

where Nu is Nusselt number; k_a is the thermal conductivity of air in the air gap, W/(m·K); d_{gp} is the thickness of the air gap, m; ξ is the packing factor of PV module; ε_{PV} and ε_{TPT} respectively represent the emissivity of the PV cell and black TPT.

The Nusselt number for a rectangular enclosure can be derived as [37]:

$$Nu = \begin{cases} 1+1.44\left(1-\dfrac{1708\cdot(\sin 1.8\varphi)^{1.6}}{Ra\cdot\cos\varphi}\right)\left[1-\dfrac{1708}{Ra\cdot\cos\varphi}\right]^{+}+\left[\left(\dfrac{Ra\cdot\cos\varphi}{5830}\right)^{1/3}-1\right]^{+}, & \text{if } T_{\mathrm{g}}<T_{\mathrm{p}} \\ 1+\left[0.364\dfrac{l_{\mathrm{p}}}{d_{\mathrm{gp}}}Ra^{1/4}-1\right]\sin\varphi, \quad \text{if } T_{\mathrm{g}}>T_{\mathrm{p}} & \\ 0, \quad \text{if } T_{\mathrm{g}}=T_{\mathrm{p}} & \end{cases} \tag{5}$$

where the + exponent indicates that only positive values are used for terms within the square brackets; in case of negative values, zero is used; φ is the inclination angle of the collector, rad; Ra is the Rayleigh number, and l_{p} refers to the length of the panel, m.

The equivalent absorptivity of the glazing cover is calculated by [38]:

$$\alpha_{\mathrm{e\_c}}=\alpha_{\mathrm{c}}+\frac{\alpha_{\mathrm{c}}\tau_{\mathrm{c}}\left[1-\alpha_{\mathrm{e\_PV}}\right]}{1-\rho_{\mathrm{c}}\left[1-\alpha_{\mathrm{e\_PV}}\right]} \tag{6}$$

where α_{c}, ρ_{c}, and τ_{c} are the absorptivity, reflectance, and transmittance of the cover, correspondingly. and $\alpha_{\mathrm{e\_PV}}$ represents the absorptivity of the PV layer, respectively, and is calculated as:

$$\alpha_{\mathrm{e\_PV}}=\xi\alpha_{\mathrm{PV}}+\left(1-\xi\right)\alpha_{\mathrm{TPT}} \tag{7}$$

where α_{PV} and α_{TPT} are the absorptivity of the solar cells and black TPT, respectively.

3.2 PV layer

The energy-balance equation of the PV layer is written as:

$$\rho_{\mathrm{PV}}c_{\mathrm{PV}}d_{\mathrm{PV}}\frac{\partial T_{\mathrm{PV}}}{\partial t}=k_{\mathrm{PV}}d_{\mathrm{PV}}\left(\frac{\partial^2 T_{\mathrm{PV}}}{\partial x^2}+\frac{\partial^2 T_{\mathrm{PV}}}{\partial y^2}\right)+h_{\mathrm{PV,c}}\left(T_{\mathrm{c}}-T_{\mathrm{PV}}\right)+\left(T_{\mathrm{p}}-T_{\mathrm{PV}}\right)/R_{\mathrm{PV,p}}+\left(\tau\alpha\right)_{\mathrm{PV}}G-\xi E_{\mathrm{PV}} \tag{8}$$

where ρ_{PV}, c_{PV}, d_{PV}, and k_{PV} denote the density, specific heat capacity, thickness, and thermal conductivity of the PV module, kg/m^3, J/(kg·K), m, and W/(m·K), correspondingly; y is the width direction of the PV/T collector, m; T_{p} is the temperature of the aluminium substrate, K; $R_{\mathrm{PV,p}}$ is the thermal resistance between the PV layer and aluminium substrate, (m^2·K)/W; $(\tau\alpha)_{\mathrm{PV}}$ is the effective transmittance–absorptivity product of the PV layer; and E_{PV} is the electrical power produced by the PV module, W/m^2.

The thermal resistance between the PV layer and aluminium substrate (i.e., the adhesive layer, a glue layer of ethylene–vinyl–acetate) is written as:

$$R_{\mathrm{PV,p}} = \frac{d_{\mathrm{PV,p}}}{k_{\mathrm{PV,p}}} \tag{9}$$

where $d_{\mathrm{PV,p}}$ and $k_{\mathrm{PV,p}}$ are the thickness and the thermal conductivity of the adhesive layer, m and W/(m·K), respectively.

The effective transmittance–absorptivity product of the PV layer is derived as:

$$(\tau\alpha)_{\mathrm{PV}} = \frac{\tau_{\mathrm{c}}\alpha_{\mathrm{e\_PV}}}{1-\left[1-\alpha_{\mathrm{e\_PV}}\right]\rho_{\mathrm{c}}} \tag{10}$$

The output electrical power of the PV/T collector is expressed as [39]:

$$E_{\mathrm{PV}} = G\tau_{\mathrm{c}}\eta_{\mathrm{ref}}\left[1+B_r\left(T_{\mathrm{PV}}-T_{\mathrm{ref}}\right)\right] \tag{11}$$

where η_{ref} is the reference efficiency of the PV module at 25 °C; and B_r is the temperature coefficient of the PV cell, and equals to –0.0045 K^{-1} for the mono-crystalline silicon solar cell.

3.3 Aluminium substrate

The energy-balance equation of the aluminium substrate is written as:

$$\rho_{\mathrm{p}}c_{\mathrm{p}}d_{\mathrm{p}}\frac{\partial T_{\mathrm{p}}}{\partial t} = k_{\mathrm{p}}d_{\mathrm{p}}\left(\frac{\partial^2 T_{\mathrm{p}}}{\partial x^2}+\frac{\partial^2 T_{\mathrm{p}}}{\partial y^2}\right)+\left(T_{\mathrm{PV}}-T_{\mathrm{p}}\right)/R_{\mathrm{PV,p}}+\frac{w_{\mathrm{p}}-N_{\mathrm{t}}D_{\mathrm{t,o}}}{w_{\mathrm{p}}}h_{\mathrm{p,b}}\left(T_{\mathrm{b}}-T_{\mathrm{p}}\right)-Q_{\mathrm{p,t}} \tag{12}$$

where ρ_{p}, c_{p}, d_{p}, and k_{p} refer to the density, specific heat capacity, thickness, and thermal conductivity of the aluminium substrate, kg/m^3, J/(kg·K), m, and W/(m·K), respectively; w_{p} is the width of the aluminium substrate, m; N_{t} is the number of copper pipes; $D_{\mathrm{t,o}}$ is the outer diameter of the pipe, m; $h_{\mathrm{p,b}}$ is the combined convective and radiative heat transfer coefficient between the aluminium substrate and the backside thermal insulation, W/(m^2·K); T_{b} is the temperature of the backside thermal insulation, K; and $Q_{p,t}$ is the heat flux between the aluminium substrate and the copper pipe, W/m^2.

The combined convective and radiative heat transfer coefficient between the aluminium substrate and backside thermal insulation is derived as [36]:

$$\begin{aligned} h_{p,b} &= h_{conv\_p,b} + h_{rad\_p,b} \\ &= \frac{Nu \cdot k_a}{d_{p,b}} + \sigma\left(T_p^2 + T_b^2\right)\left(T_p + T_b\right)\frac{1}{1/\varepsilon_p + 1/\varepsilon_b - 1} \end{aligned} \tag{13}$$

where $d_{p,b}$ is the thickness between the aluminium substrate and backside thermal insulation, m; and ε_p and ε_b are the emissivity of the aluminium substrate and backside thermal insulation, correspondingly.

The heat transfer between the aluminium substrate and the copper pipe only takes place where the two components are connected, and thus the heat transfer flux is expressed as:

$$Q_{p,t} = \begin{cases} (T_p - T_t)\big/\left(R_{p,t} \cdot A_{ij}\right), & \text{connected sections} \\ 0, & \text{disconnected sections} \end{cases} \tag{14}$$

where A_{ij} denotes the area of a control volume, m^2; and $R_{p,t}$ is the thermal resistance between the aluminium substrate and each copper pipe, K/W, and is derived as:

$$R_{p,t} = \frac{d_{p,t}}{k_{p,t} A_{p,t}} \tag{15}$$

where $d_{p,t}$, $k_{p,t}$, and $A_{p,t}$ are the thickness, thermal conductivity, and joint area of the aluminium substrate and each copper pipe, m, W/(m·K), and m^2, correspondingly.

3.4 Copper pipe

The energy-balance equation of the copper pipe is presented as:

$$\rho_t c_t \pi \frac{D_{t,o}^2 - D_{t,i}^2}{4}\frac{\partial T_t}{\partial t} = \pi \frac{D_{t,o}^2 - D_{t,i}^2}{4} k_t \frac{\partial^2 T_t}{\partial x^2} + \pi D_{t,i} h_{w,t}\left(T_w - T_t\right) + \frac{T_p - T_t}{R_{p,t} \cdot dx} + D_{t,o} h_{t,b}\left(T_b - T_t\right) \tag{16}$$

where ρ_t, c_t, d_t, and k_t refer to the density, specific heat capacity, thickness, and thermal conductivity of the copper pipe, kg/m^3, J/(kg·K), m, and W/(m·K), correspondingly; T_t and T_w are the temperatures of the pipe and water in the pipe, K, respectively; $D_{\mathrm{t,i}}$ is the inner diameter of the copper pipe, m; $h_{\mathrm{w,t}}$ is the convective heat transfer coefficient between the copper pipe and the inner water flow, W/(m^2·K); and $h_{\mathrm{t,b}}$ is the heat transfer coefficient between the copper pipe and the backside thermal insulation, W/(m^2·K), and is the same to the $h_{\mathrm{p,b}}$ for simplicity.

3.5 Water in the copper pipe

The energy-balance equation of the water in the copper pipe is written as:

$$\frac{\rho_{\mathrm{w}} c_{\mathrm{w}} \pi D_{\mathrm{i}}^2}{4} \frac{\partial T_{\mathrm{w}}}{\partial t} = -\dot{m} c_{\mathrm{w}} \frac{\partial T_{\mathrm{w}}}{\partial x} + \frac{\pi D_{\mathrm{i}}^2}{4} k_{\mathrm{w}} \frac{\partial^2 T_{\mathrm{w}}}{\partial x^2} + P_{\mathrm{t}} h_{\mathrm{w,t}} \left(T_{\mathrm{t}} - T_{\mathrm{w}}\right) \tag{17}$$

where ρ_{w} and c_{w} are the density and the specific heat capacity of water in the pipe, kg/m^3 and J/(kg·K), correspondingly; $\dot{m}$ is the mass flow rate of water in each pipe, kg/s; and P_{t} is the inner perimeter of the copper pipe, m.

3.6 Backside thermal insulation

The energy-balance equation of the backside thermal insulation is expressed as:

$$\rho_{\mathrm{b}} c_{\mathrm{b}} d_{\mathrm{b}} \frac{\partial T_{\mathrm{b}}}{\partial t} = k_{\mathrm{b}} d_{\mathrm{b}} \frac{\partial^2 T_{\mathrm{b}}}{\partial x^2} + \frac{w_{\mathrm{p}} - N_{\mathrm{t}} D_{\mathrm{t,o}}}{w_{\mathrm{p}}} h_{\mathrm{p,b}} \left(T_{\mathrm{p}} - T_{\mathrm{b}}\right) + \frac{N_{\mathrm{t}} D_{\mathrm{t,o}}}{w_{\mathrm{p}}} h_{\mathrm{t,b}} \left(T_{\mathrm{t}} - T_{\mathrm{b}}\right) + U_{\mathrm{a,b}} \left(T_{\mathrm{a}} - T_{\mathrm{b}}\right) \tag{18}$$

where ρ_{b}, c_{b}, d_{b}, and k_{b} denote the density, specific heat capacity, thickness, and thermal conductivity of the upper surface of the backside thermal insulation, kg/m^3, J/(kg·K), m, and W/(m·K), respectively; and $U_{\mathrm{a,b}}$ is the overall coefficient of heat transfer between the upper surface of the backside thermal insulation and local outside environment, W/(m^2·K), and is calculated as:

$$U_{\mathrm{a,b}} = \frac{1}{R_{\mathrm{b}} + 1/h_{\mathrm{a,b}}} = \frac{1}{d_{\mathrm{b}}/k_{\mathrm{b}} + 1/h_{\mathrm{a,b}}} \tag{19}$$

where R_{b} denotes the thermal resistance of the backside thermal insulation, K/W; and $h_{\mathrm{a,b}}$ represents the convective heat transfer coefficient between the backside thermal insulation and ambient air, W/(m^2·K), and is the same to the $h_{\mathrm{a,c}}$ in expression.

3.7 Water tank

The energy-balance equation of the water tank is written as:

$$A_{\mathrm{tank}}\rho_{\mathrm{w}}c_{\mathrm{w}}\frac{\partial T_{\mathrm{tank}}}{\partial t}=-\dot{M}c_{\mathrm{w}}\frac{\partial T_{\mathrm{tank}}}{\partial z}+A_{\mathrm{tank}}k_{\mathrm{w}}\frac{\partial^{2}T_{\mathrm{tank}}}{\partial z^{2}}+P_{\mathrm{tank}}U_{\mathrm{a,tank}}\left(T_{\mathrm{a}}-T_{\mathrm{tank}}\right) \tag{20}$$

where A_{tank} represents the inner cross-sectional area of the water tank, m^2; T_{tank} is the temperature of water in the tank, K; $\dot{M}$ is the mass flow rate of water in the tank, kg/s; z is the height direction of the water tank, m; P_{tank} is the outer perimeter of the water tank, m; and $U_{\mathrm{a,tank}}$ is the overall coefficient of heat transfer between water in the tank and ambient air, W/(m^2·K), and is expressed as:

$$U_{\mathrm{a,tank}}=\frac{1}{\dfrac{D_{\mathrm{tank,o}}}{2k_{\mathrm{tank}}}\ln\dfrac{D_{\mathrm{tank,o}}}{D_{\mathrm{tank,i}}}+\dfrac{1}{h_{\mathrm{a,tank}}}} \tag{21}$$

where $D_{\mathrm{tank,i}}$ and $D_{\mathrm{tank,o}}$ refer to the inner and outer diameters of the water tank, correspondingly, m; k_{tank} is the thermal conductivity of the tank wall, W/(m·K); and $h_{\mathrm{a,tank}}$ is the convective heat transfer coefficient between the ambient air and water in the tank, W/(m^2·K).

3.8 performance evaluation

The average electrical efficiency of the PV/T system over the simulated operation period is calculated as:

$$\overline{\eta_{\mathrm{e}}}=\sum\frac{UI\Delta t}{GA_{\mathrm{PV}}\Delta t}=\frac{\sum UI\Delta t}{10^{6}HA_{\mathrm{PV}}} \tag{22}$$

where Δt refers to the time step, s; H is the total solar radiation received over the simulated operation period, MJ/m^2, and A_{PV} is the total area of the PV cells in the PV layer, m.

The average thermal efficiency of the PV/T system over the simulated operation period is derived as:

$$\overline{\eta_{\mathrm{th}}}=\frac{S_{\mathrm{th}}}{HA_{\mathrm{p}}}=\frac{mc_{\mathrm{w}}\left(T_{\mathrm{final}}-T_{\mathrm{initial}}\right)}{10^{6}HA_{\mathrm{p}}} \tag{23}$$

where S_{th} denotes the total heat gain of water in the tank, MJ; m denotes the mass of water in the tank, kg; and $T_{initial}$ and T_{final} represent the initial and final water temperatures in the water tank, respectively, K.

The total efficiency of the PV/T system is defined as the sum of the electrical and thermal efficiencies [40]:

$$\overline{\eta_{total}} = \overline{\eta_e} + \overline{\eta_{th}} \tag{24}$$

3.9 Discretization

The energy-balance equation of different components of the E-PV/T system is discretized using the finite difference method. Fig. 4 shows the Space discretization of the PV layer and aluminium substrate of the E-PV/T collector. As the temperature field of the PV layer and aluminium substrate is periodic along the y-direction and symmetric along each copper pipe in the x-direction, only half the area between two copper pipes with symmetric boundary conditions on both sides of the y-direction is determined as the calculation area of the PV layer and aluminium substrate. 41 nodes along the x-direction and 6 nodes along the y-direction are set uniformly to divide the temperature field of the PV layer and aluminium substrate. For the seven copper pipes and working fluid in each copper tube, 39 nodes along the x-direction are set relative to the aluminium substrate. For the glazing cover and backside thermal insulation, however, 41 nodes along the x-direction are set correspondingly.

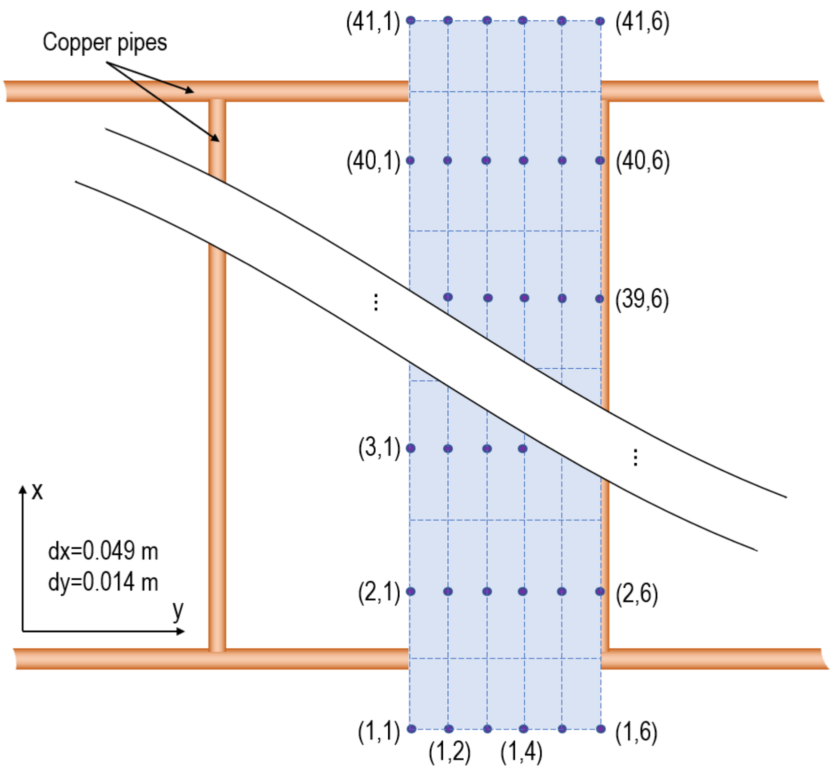

Fig. 4. Space discretization of the PV layer and aluminium substrate of the E-PV/T collector.

A MATLAB computational program is developed based on the above mathematic model and discrete method to characterize the performance of the E-PV/T system operating in different conditions. The calculation flow chart of the simulation program is shown in Fig. 5.

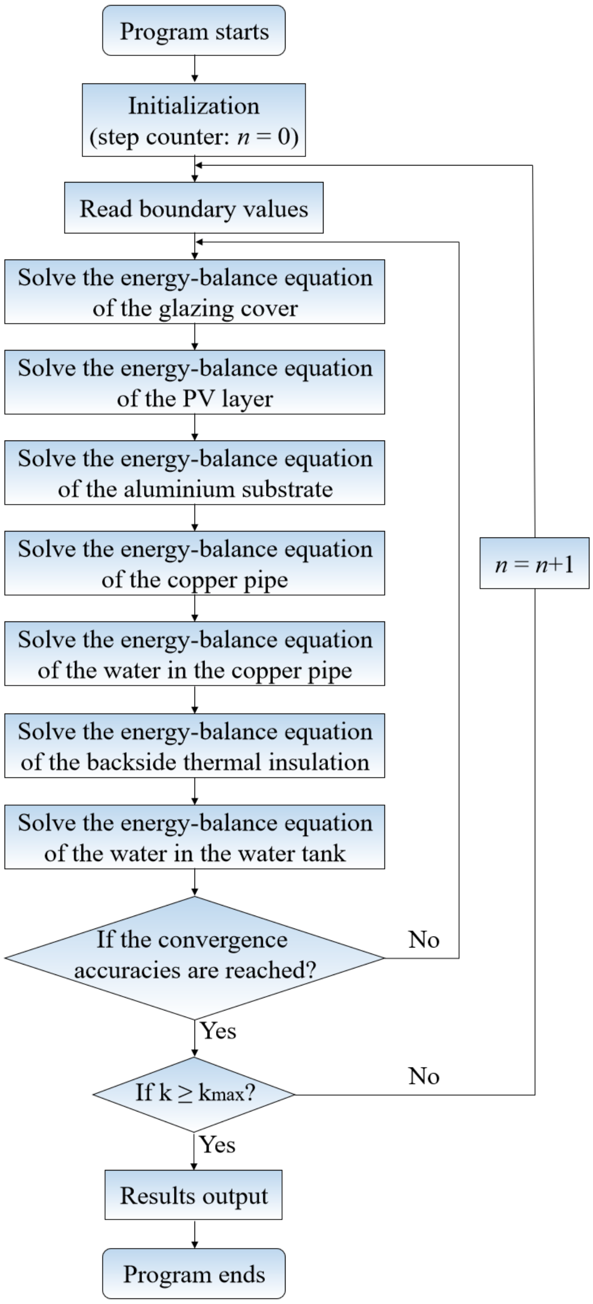

Fig. 5. Calculation flow chart of the simulation program.

4. Results and discussion

Based on the mathematic model and MATLAB coding developed in Section 3, a comprehensive numerical study is carried out to evaluate the performance of the E-PV/T system and its performance is compared with that of the N-PV/T system with the same size. Besides, the effect of some key parameters on the output performance of the E-PV/T system is characterized as well.

4.1. Model validation

Firstly, the mathematic model developed in Section 3 is validated using experimental results derived from a previous research on the N-PV/T collector developed by the authors [35]. This N-PV/T collector is structurally quite the same as the E-PV/T collector proposed in this study except for the vacuum circumstance in the two inner spaces, namely, the upper and lower spaces. The two inner spaces in the previous study took no specific vacuuming while assumed to be vacuumed to certain degrees in this study. Therefore, the mathematic model for performance characterization of the N-PV/T and E-PV/T collectors are the same except the value of convective heat transfer coefficient in the upper and lower spaces are different in the two collectors. This difference will not affect the reasonability of using the measured data of the N-PV/T collector to validate the mathematic model developed in Section 3. The structural parameters of the N-PV/T collector are listed in Table 1. To quantificationally assess the differentials between the experimental and simulated results, the equations of mean relative error (MRE) are adopted as follows [41]:

$$\mathrm{MRE} = \frac{1}{n}\sum_{i=1}^{i=n}\left|\frac{X_{\exp,i} - X_{\mathrm{sim},i}}{X_{\exp,i}}\right| \times 100\% \tag{25}$$

where $X_{\exp,i}$ and $X_{\mathrm{sim},i}$ respectively denote the i^{th} experimental and simulation values, and n represents the number of experimental data.

Table 1. Structural parameters of the N-PV/T collector.

Components	Parameters	Values
Glazing cover	Aperture area	1.893 m^2
	Emissivity	0.88
	Thermal conductivity	1.05 W/(m·K)
	Heat capacity	750 J/(kg·K)
	Thickness	0.0032 m
	Density	2500 kg/m^3
PV module	Area	1.12 m^2
	Absorptivity	0.95

	Emissivity	0.95
	Reference efficiency	0.135
	Thermal conductivity	149 W/(m·K)
	Heat capacity	700 J/(kg·K)
	Thickness	0.0006 m
	Density	600 kg/m^3
Aluminium substrate	Emissivity (upper surface)	0.95
	Emissivity (lower surface)	0.1
	Thermal conductivity	237 W/(m·K)
	Heat capacity	903 J/(kg·K)
	Thickness	0.001 m
	Density	2702 kg/m^3
Copper pipes	External diameter	0.01 m
	Internal diameter	0.008 m
	Number	7
	Thermal conductivity	393 W/(m·K)
	Heat capacity	385 J/(kg·K)
	Density	8933 kg/m^3
Backside thermal insulation	Emissivity (upper surface)	0.1
	Thermal conductivity	0.046 W/(m·K)
	Heat capacity	670 J/(kg·K)
	Thickness	0.03 m
	Density	30 kg/m^3
Air gap	Height	0.03 m

Specifically, the experimental results of the N-PV/T collector from 12:00 to 14:30 on 11th December 2013 in Hefei, China are employed to validate the mathematic model. Fig. 6 illustrates the solar irradiance and ambient temperature during the experimental period. As shown in Fig. 7, a high degree of consistency is observed between the experimental and simulated results in terms of instantaneous electrical power and water temperature in the water tank that respectively represent the instantaneous electrical and thermal performance. The RME for the electrical power, water temperature in the tank (in Celsius scale), and water temperature rise through the collector is 6.04%, 0.33%, and 8.57%, respectively, indicating that the developed mathematic model can be employed to predict the electrical and thermal performance of the N-PV/T and E-PV/T systems. Moreover, Table 2 further presents the experimental and simulation results of the overall performance indicators.

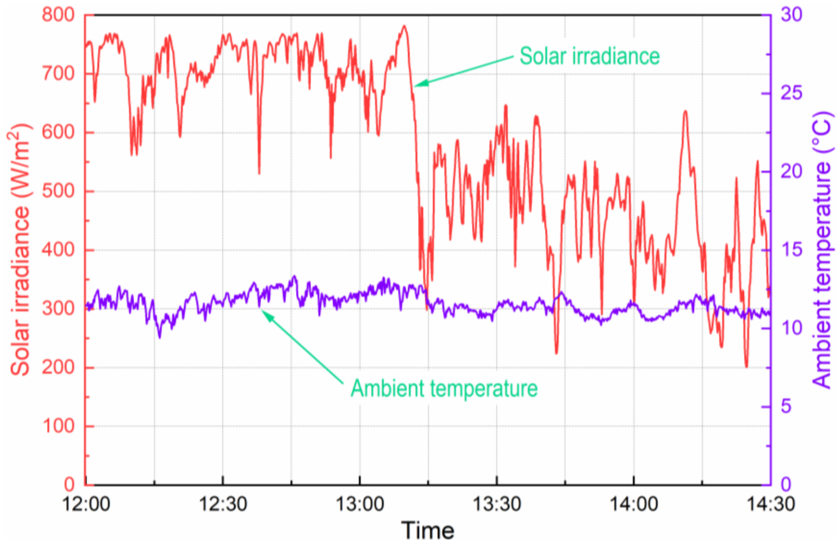

Fig. 6. The solar irradiance and ambient temperature during the experimental period (from 12:00 to 14:30 on 11th December 2013) in Hefei, China.

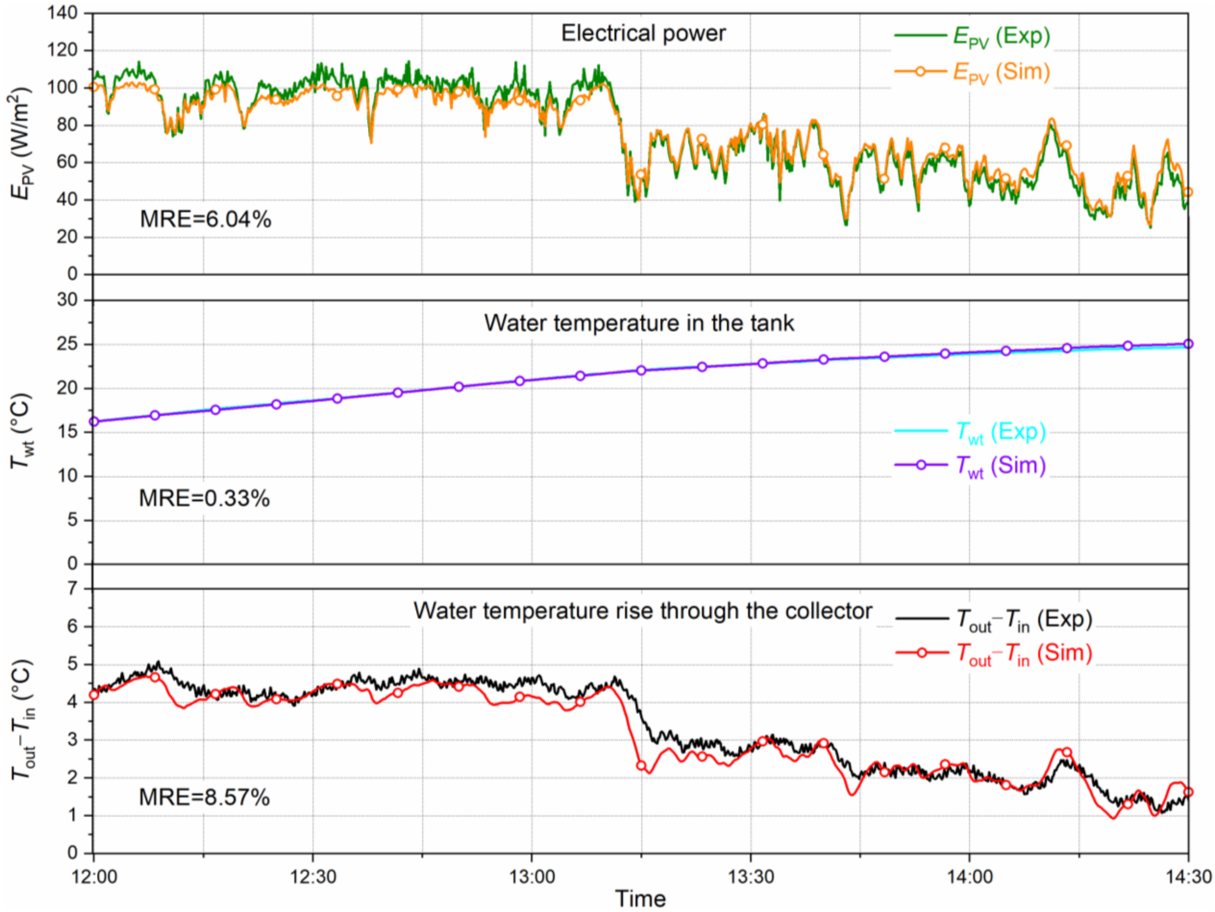

Fig. 7. Simulated electrical power, water temperature in the tank, and outlet-inlet water temperature difference compared to the experimental data on 11th December 2013 in Hefei, China.

Table 2. Experimental and simulation results of the overall performance indicators of the N-PV/T system.

Indicators	Experimental results	Simulation results
Total electricity output	192.73 Wh	193.75 Wh
Total heat gain in the tank	4.26 MJ	4.36 MJ
Final water temperature in the tank	24.68 °C	24.91 °C
Electrical efficiency	11.75%	11.98%
Thermal efficiency	43.22%	44.01%
Total efficiency	54.97%	55.99%

4.2. Parametric study

Based on the experimentally validated mathematic model, the effect of some key parameters on the performance of the E-PV/T collector is investigated. The weather parameters involved in the parametric study (e.g., ambient air temperature, solar irradiance, wind velocity) are adopted from the in-situ measured data from 8:00 to 16:00 on 18th April 2018 in Hefei, China, as shown in Fig. 8. The ambient air temperature and solar irradiance were recorded every 10 seconds using a thermocouple located in a thermometer shelter and a pyranometer, respectively, and the wind velocity was measured every 10 minutes using an automatic meteorological station.

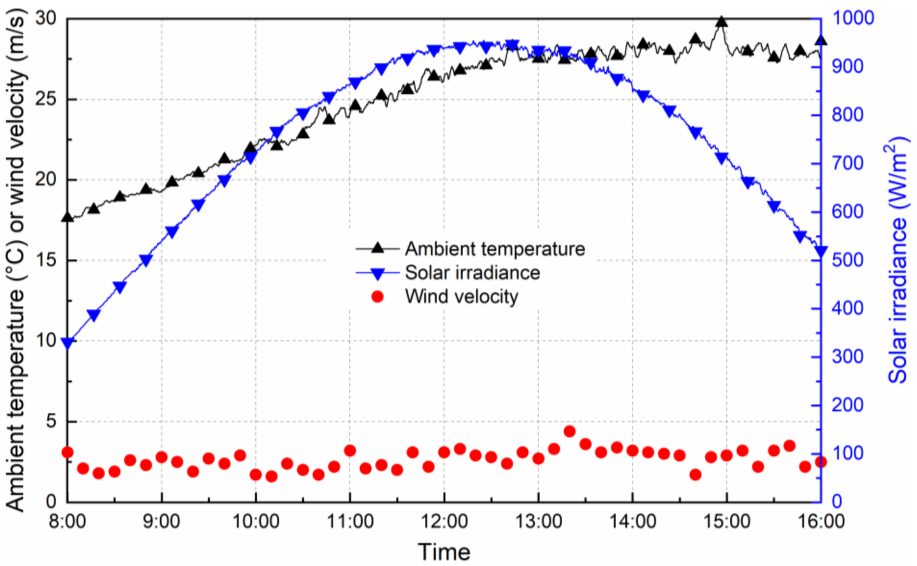

Fig. 8. The measured weather data from 8:00 to 16:00 on 18th April 2018 in Hefei, China (The ambient temperature and solar irradiance were recorded every 10 seconds, and the wind velocity was measured every 10

minutes).

4.2.1 Performance enhancement in low-temperature conditions owing to vacuum

Firstly, the performance enhancement benefited from the vacuum design in low-temperature conditions is investigated. The initial water temperature in the water tank (hereafter referred to as the "initial water temperature") is set equal to the initial ambient temperature, 17.6 °C. As shown in Fig. 9, not much difference is observed between the performance of the E-PV/T and N-PV/T system during the whole simulation period. Due to the vacuum around, the panel temperature of the E-PV/T collector is always a little higher than that of the N-PV/T collector, resulting in a tiny lower electrical power of the PV module and a slightly higher water temperature in the water tank. Further refer to Table 3, the final water temperature in the water tank of the E-PV/T system is only about 3.1 °C higher than that of the N-PV/T system, indicating that the thermal performance improvement attributed to the vacuum structure is not distinct in low-temperature cases. This is because the vacuum design can only suppress the non-radiative (i.e., conductive and convective) heat loss of the PV/T collector, but the radiative heat loss takes a sizeable share of the overall heat loss of the collector when the panel temperature is relatively low. Considering the cost of creating a vacuum local environment within the PV/T collector, though the vacuum scheme can always increase the thermal efficiency of the PV/T collector, it doesn't make much sense to employ such an E-PV/T collector for low-temperature applications such as domestic hot water supplying for which around 50 ℃ water is enough.

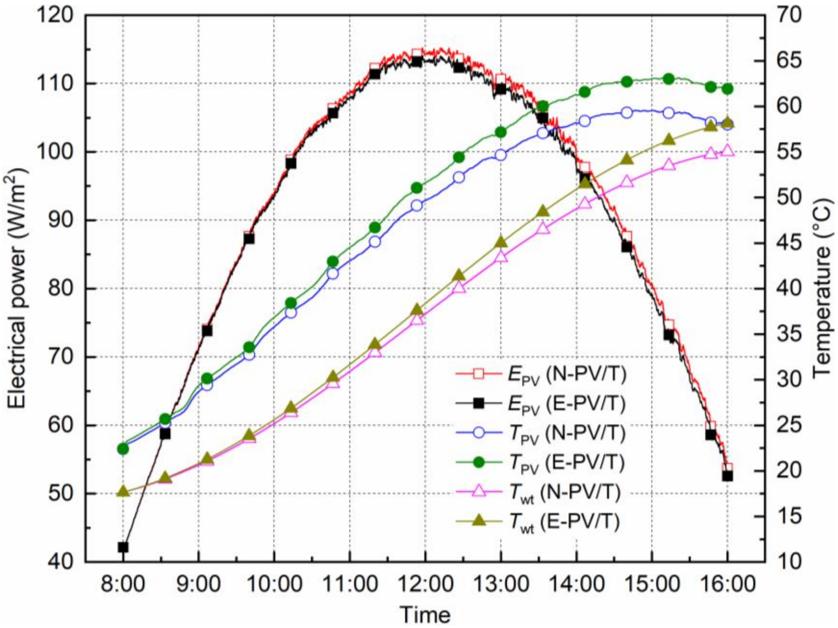

Fig. 9. The electrical power, panel temperature, and water temperature in the water tank of the E-PV/T and N-PV/T systems (Initial water temperature equals the initial ambient temperature, 17.6 °C).

Table 3. The final performance indicators of the E-PV/T and N-PV/T systems working in low-temperature. conditions.

Indicators	E-PV/T system	N-PV/T system
Total electricity output	726.34 Wh	734.17 Wh
Total heat gain in the tank	20.41 MJ	18.84 MJ
Final water temperature in the tank	58.13 ℃	55.02 ℃
Electrical efficiency	10.73%	10.85%
Thermal efficiency	49.56%	45.76%
Total efficiency	60.29%	56.61%

4.2.2. Performance in different temperature conditions

The performance improvement of the E-PV/T system is proved to be not obvious compared to the N-PV/T system in low-temperature working conditions, yet the performance of the E-PV/T system operating in higher temperatures is not clear. Therefore, further study is conducted to explore the performance profile of the E-PV/T system working in a wide range of temperature conditions, as the results shown in Fig. 10. It is clear from Fig. 10(a) that the water temperature increment in the water tank of both systems declines gradually as the initial water temperature increases and the temperature gap between the two systems is larger at greater initial water temperature. In addition, the temperature increment in the water tank of the N-PV/T system drops to zero when the initial water temperature increases to about 85 °C, while that of the E-PV/T system can still reach about 8 °C, with the thermal efficiency being 9.81% in this case. According to Fig. 10(b), the daily thermal efficiency of the two systems can be linearly fitted and expressed as:

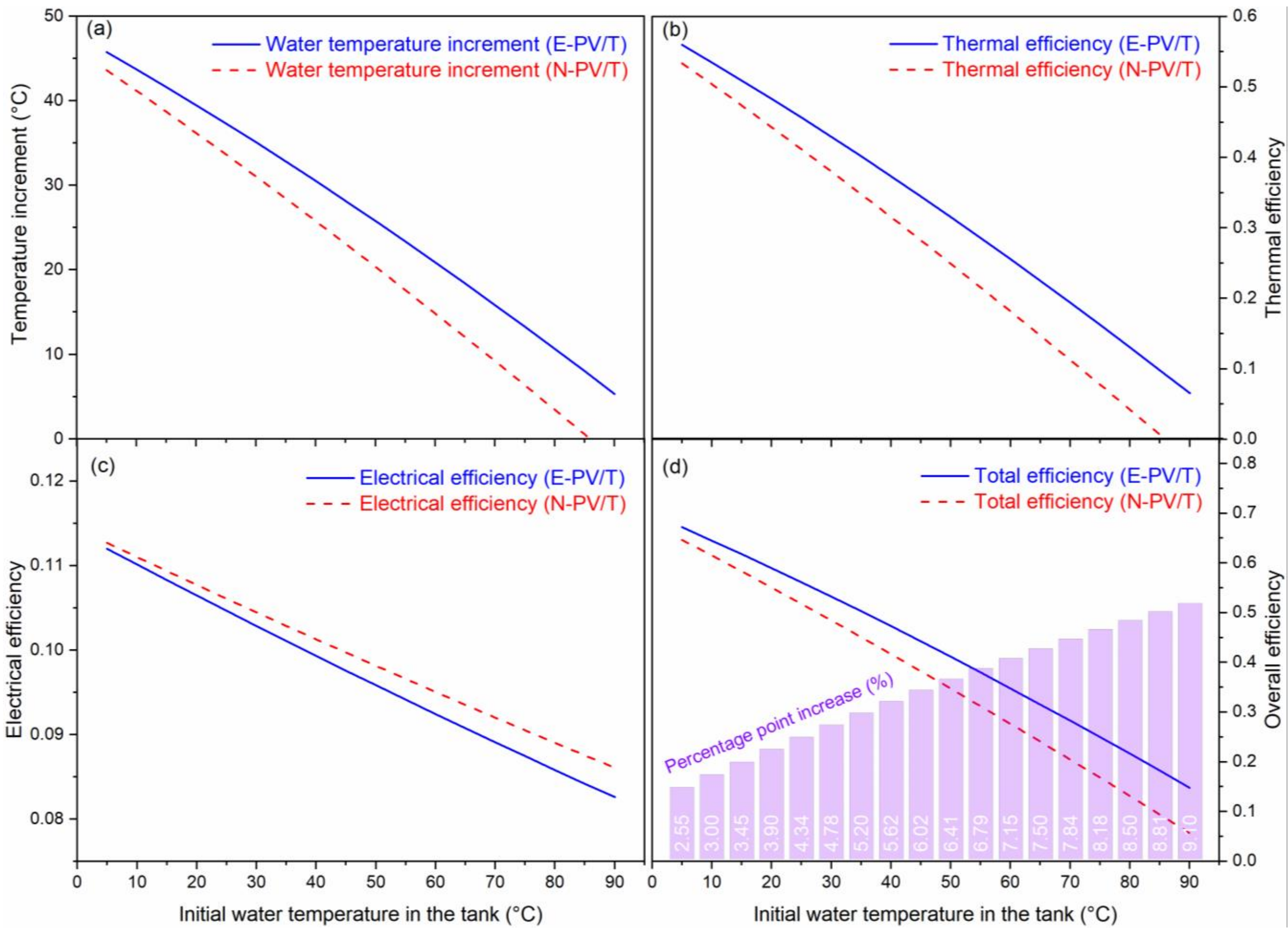

Fig. 10. The effect of the initial water temperature on the water temperature increment and thermal efficiencies of the E-PV/T and N-PV/T systems.

$$\overline{\eta_{\text{th\_E-PV/T}}} = 0.457 - \frac{0.117}{H}\left(T_{\text{initial}} - \overline{T}_{\text{a}}\right) - \frac{0.000211}{H}\left(T_{\text{initial}} - \overline{T}_{\text{a}}\right)^2 \tag{26}$$

$$\overline{\eta_{\text{th\_N-PV/T}}} = 0.412 - \frac{0.137}{H}\left(T_{\text{initial}} - \overline{T}_{\text{a}}\right) - \frac{0.000162}{H}\left(T_{\text{initial}} - \overline{T}_{\text{a}}\right)^2 \tag{27}$$

Based on the two regression equations, the thermal performance of the E-PV/T and N-PV/T systems under certain weather conditions and initial water temperature can be predicted and compared. The thermal efficiency at zero-reduced temperature is 45.7% for the E-PV/T system, which is about 10.9% higher than that of the N-PV/T system.

From Fig. 10(c), on the other hand, the electrical efficiency of the E-PV/T system becomes increasingly lower than that of the N-PV/T system at elevated initial water temperature. This is because the average panel temperature difference between the two systems is greater at higher-temperature conditions and thus resulting in enlarged PV performance difference between the two systems. Nevertheless, the total efficiency of the E-PV/T system benefits from the vacuum, especially at high-temperature levels. For instance, the absolute total efficiency improvement of the E-PV/T system, compared to that of the N-PV/T system, goes up from 2.55% to 9.10% as the initial water temperature increases from 5 °C to 90 °C.

4.2.3. Effect of the vacuum degree

The two inner spaces, namely, the upper and lower spaces, are vacuumed to eradicate the non-radiative heat loss of the absorber panel, yet it is difficult to keep the two spaces being ideally vacuum, especially after a long-term operation without any additional vacuum treatment. Therefore, the effect of the vacuum degree of the two inner spaces on the performance of the E-PV/T collector is further investigated. In the present study, the vacuum degree is confirmed as 0% if the inner space is completely non-vacuumed and 100% if is ideally vacuumed. Fig. 11 illustrates the final water temperature in the water tank and output efficiencies of the E-PV/T system under different vacuum degrees. The vacuum degree of the upper space exerts a greater influence on the performance of the E-PV/T system compared to that of the lower space. For the upper space the absorber panel is the hot and bottom surface relative to the glazing cover, while for the lower space the absorber panel is the hot but top surface with respect to the backside thermal insulation. Therefore, the free convection that occurred in the upper space is more intense compared to that in the lower space, revealing that more attention should be paid to the vacuum of the upper space in the E-PV/T collector. In the present study, the initial water temperature is set at 80 °C to make the E-PV/T collector working in a typical high-temperature operation condition. When the vacuum degree of the upper space decreases from 100% to 0%, the electrical efficiency increases from 8.55% to 8.82%, while the thermal and total efficiencies decrease from 13.50% and 26.82% to 6.38% and 20.10%, correspondingly. By contrast, as the vacuum degree of the lower space degrades from 100% to 0%, the three key indicators change slightly to 8.62%, 11.49%, and 24.91%, respectively. As the vacuum degree of the lower space exerts marginal effects on the performance of the E-PV/T collector, this space can be handled as a non-vacuum cavity to save the cost of vacuuming. Furthermore, the lower space can be arranged as an air duct to extend the PV/T collector to be a solar air heater meanwhile if hot air is needed.

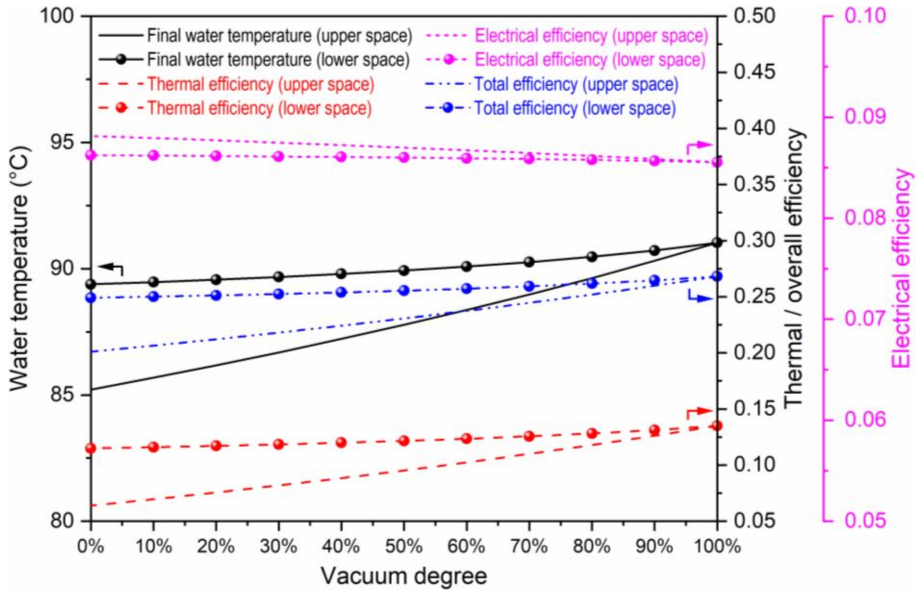

Fig. 11. The final water temperature in the water tank and output efficiencies of the E-PV/T system under different vacuum degrees. (Initial water temperature is set at 80 °C).

4.2.4. Effect of the long-wave panel emissivity

Although it is proved that the vacuum structure can improve the thermal performance of the flat-plate PV/T collector and make possible its operation at initial water temperature over 90 °C, the thermal efficiency of the E-PV/T system is still not very desirable. Regardless of a part of the incident solar energy is converted into electricity, another reason that causes the relatively low thermal efficiency of an E-PV/T collector is its high panel emissivity in the middle- and far-infrared bands. Lower infrared panel emissivity stands for lower long-wave radiative heat loss and thus higher thermal efficiency, as the results shown in Fig. 12. Though the electrical efficiency shows an opposite changing trend to the thermal efficiency, the total efficiency increases rapidly as the long-wave panel emissivity decreases. Specifically, the thermal and total efficiencies of the E-PV/T system are respectively 13.50% and 26.82% when the long-wave panel emissivity is 0.95, but these indicators increase dramatically to 49.78% and 61.20% correspondingly when the long-wave panel emissivity is only 0.05. It may be unrealistic to prepare a PV/T panel with such a low emissivity, but it is possible to get a PV/T panel with a moderate long-wave emissivity such as 0.4 to 0.5, under which situations the E-PV/T system still shows quite favorable thermal and total efficiencies. For instance, the total efficiency of the E-PV/T system reaches 41.27% when the long-wave panel emissivity is 0.4. Therefore, it will be an interesting strategy to develop spectrally selective PV/T panels (high solar absorption and low long-wave emission) for thermal performance improvement of a PV/T collector. The booming developments in micro- and nano-material technologies may offer many possibilities for such an innovation.

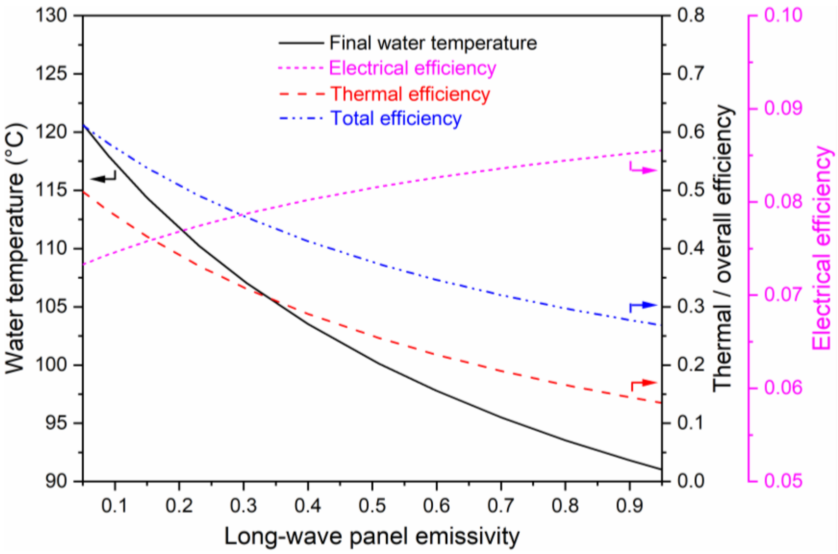

Fig. 12. The final water temperature in the water tank and output efficiencies of the E-PV/T system under different long-wave (above 3 μm) panel emissivity. (Initial water temperature is set at 80 °C).

4.2.5. Effect of the temperature coefficient of PV cells

The electrical efficiency of the E-PV/T system deteriorates at elevated panel temperatures, which is resulted from the negative temperature coefficient effect of mono-crystalline silicon solar cells. Therefore, an increment in thermal efficiency will inevitably bring a side-effect of electrical performance deterioration. The temperature coefficient of PV cells employed in this study is about –0.0045 K^{-1}. If higher electrical performance is pursued in high-temperature scenarios, developing new PV cells with lower temperature coefficients will make sense. Fig. 13 illustrates the performance of the E-PV/T system under different temperature coefficients of the PV cell. The electrical efficiency increases linearly from 8.55% to 11.32% as the temperature coefficient decreases from –0.0045 to –0.001 K^{-1} [42, 43]. Though the thermal efficiency decreases to a small extent, the total efficiency is enhanced from 26.82% to 30.16%. Regardless of the intrinsic PV conversion efficiency, solar cells with negative temperature coefficient closer to zero (e.g., amorphous silicon cell [44]) or even positive temperature coefficient (e.g., nonpolar InGaN cell [42]) are particularly appealing for high-temperature solar PV/T installations, including the E-PV/T collector in this study.

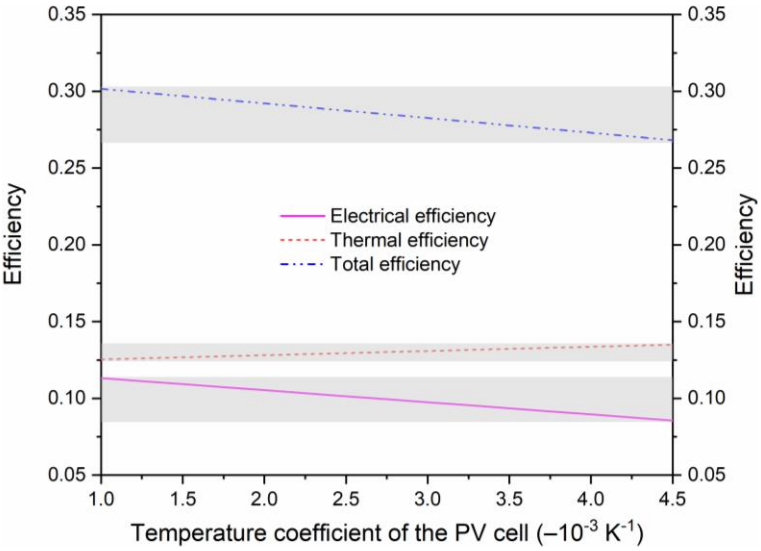

Fig. 13. The output efficiencies of the E-PV/T system under different temperature coefficients of the PV cell.

(Initial water temperature is set at 80 °C and long-wave panel emissivity is set at 0.95).

5. Conclusions

In the present study, a novel evacuated flat-plate PV/T (E-PV/T) collector is proposed in order to improve its thermal performance and effectively run it in high-temperature conditions. A dynamic-state mathematic model is developed to assess the output performance of the E-PV/T system under different working conditions. The detailed results are summarized as follows:

(1) The thermal performance improvement benefitted from the vacuum design is not distinct in low-temperature conditions, with only 3.8 percentage points increment when the initial water temperature in the tank is equal to the initial ambient temperature, 17.6 °C.

(2) Comparing to the N-PV/T system, the percentage point increase of the total efficiency of the E-PV/T system elevates from 2.55% to 9.10% as the initial water temperature in the water tank increases from 5 °C to 90 °C.

(3) The electrical, thermal, and total efficiencies of the E-PV/T system with an initial water temperature of 80 °C is respectively 8.55%, 13.50%, and 26.82%, but change to 8.82%, 6.38%, and 20.10%, respectively when the vacuum degree of the upper space declines from 100% to 0%, and change slightly to 8.62%, 11.49%, and 24.91%, correspondingly as the vacuum degree of the lower space degrades from 100% to 0%.

(4) The long-wave panel emissivity exerts a dramatic negative effect on the thermal performance of the E-PV/T system with an initial water temperature of 80 °C. Its thermal efficiency trebles from 16.9% to 54.4 % as the long-wave panel emissivity decreases from 0.95 to 0.05.

(5) The electrical and total efficiencies increase linearly from 8.55% and 26.82% to 11.32% and 30.16% as the temperature coefficient decreases from –0.0045 to –0.001 K^{-1}, with an initial water temperature of 80 °C and long-wave panel emissivity of 0.95.

Overall, the E-PV/T collector is proved to be an efficient hybrid electrical and thermal energy harvester working in high-temperature conditions. The superior of working in a wider range of temperatures enables the E-PV/T collector to be a more effective renewable energy provider in scenarios such as building, industrial, and agriculture fields. Future studies will focus on the fabrication of a practical-scale E-PV/T collector and the outdoor experimental investigation of the E-PV/T collector in different weather and operation conditions.

Acknowledgments

This study was sponsored by the National Key R&D Program of China (2018YFD0700200), H2020 Marie Skłodowska-Curie Actions - Individual Fellowships (842096), National Natural Science Foundation of China (NSFC 51906241, 51761145109, and 51776193), Anhui Provincial Natural Science Foundation (1908085ME138), and China Postdoctoral Science Foundation (2019M652209).

Nomenclature

A: area, m^2
B_r: temperature coefficient of PV cells, K^{-1}
c: specific heat capacity, J/(kg·K)
D: diameter, m
d: thickness, m
E: electrical power, W/m^2
G: solar irradiance, W/m^2
H: total solar radiant energy, MJ/m^2
h: heat transfer coefficient, W/(m^2·K)
I: current, A
k: thermal conductivity, W/(m·K)
l: length, m
m: mass of water in the tank, kg
$\dot{m}$ and $\dot{M}$: mass flow rate, kg/s
N: number, -
Nu: Nusselt number, -
P: perimeter or electricity gain, m or MJ
Q: heat flux or heat gain, W/m^2 or MJ
R: thermal resistance, K/W
MRE: mean relative error, -
S: total heat gain, MJ
T: temperature, K
t: time, s
Δt: time interval, s
U: voltage or overall heat-transfer coefficient, V or W/(m^2·K)
w: width, m
x: length direction of the PV/T collector, m
y: width direction of the PV/T collector, m
z: height direction of the water tank, m
τ: transmittance, -
($\tau\alpha$): transmittance-absorptance product, -
α: absorptivity, -
ε: emissivity, -
ρ: reflectance or density, - or kg/m^3
σ: Stefan–Boltzmann constant, W/m$^2\cdot$K^4
φ: inclination angle, rad
ξ: packing factor, -
$\bar{\eta}$: daily average efficiency, -

Abbreviation and subscripts
a: ambient air

b: backside thermal insulation
c: glazing cover
conv: convective
N-PV/T: normal photovoltaic/thermal collector or system
e: electrical or equivalent
E-PV/T: evacuated photovoltaic/thermal collector or system
Exp: experiment
final: final water temperatures in the water tank
i: inner
initial: initial water temperatures in the water tank
o: outer
p: aluminium substrate
PV: PV module
rad: radiative
ref: reference
s: sky
Sim: simulation
t: copper pipe
tank: water tank
th: thermal
w: water

References

[1] N. Shao, L. Ma, J. Zhang, Experimental study on electrical and thermal performance and heat transfer characteristic of PV/T roof in summer, Applied Thermal Engineering 162 (2019) 114276.

[2] R.A. Agathokleous, S.A. Kalogirou, S. Karellas, Exergy analysis of a naturally ventilated Building Integrated Photovoltaic/Thermal (BIPV/T) system, Renewable Energy 128 (2018) 541-552.

[3] Q. Yu, M. Hu, J. Li, Y. Wang, G. Pei, Development of a 2D temperature-irradiance coupling model for performance characterizations of the flat-plate photovoltaic/thermal (PV/T) collector, Renewable Energy 153 (2020) 404-419.

[4] P. Jha, B. Das, R. Gupta, An experimental study of a photovoltaic thermal air collector (PVTAC): A comparison of a flat and the wavy collector, Applied Thermal Engineering 163 (2019) 114344.

[5] D. Das, P. Kalita, O. Roy, Flat plate hybrid photovoltaic- thermal (PV/T) system: A review on design and development, Renewable and Sustainable Energy Reviews 84 (2018) 111-130.

[6] I. Guarracino, J. Freeman, A. Ramos, S.A. Kalogirou, N.J. Ekins-Daukes, C.N. Markides, Systematic testing of hybrid PV-thermal (PVT) solar collectors in steady-state and dynamic outdoor conditions, Applied Energy 240 (2019) 1014-1030.

[7] K. Luo, J. Ji, L. Xu, Z. Li, Seasonal experimental study of a hybrid photovoltaic-water/air solar wall system, Applied Thermal Engineering 169 (2020) 114853.

[8] F. Huide, Z. Xuxin, M. Lei, Z. Tao, W. Qixing, S. Hongyuan, A comparative study on three types of solar utilization technologies for buildings: Photovoltaic, solar thermal and hybrid photovoltaic/thermal systems, Energy Conversion and Management 140 (2017) 1-13.

[9] T. Ma, M. Li, A. Kazemian, Photovoltaic thermal module and solar thermal collector connected in series to produce electricity and high-grade heat simultaneously, Applied Energy 261 (2020) 114380.

[10] M.M.A. El-Samie, X. Ju, Z. Zhang, S.A. Adam, X. Pan, C. Xu, Three-dimensional numerical investigation of a hybrid low concentrated photovoltaic/thermal system, Energy 190 (2020) 116436.

[11] X. Han, X. Zhao, X. Chen, Design and analysis of a concentrating PV/T system with nanofluid based spectral beam splitter and heat pipe cooling, Renewable Energy 162 (2020) 55-70.

[12] M. Souliotis, N. Arnaoutakis, G. Panaras, A. Kavga, S. Papaefthimiou, Experimental study and Life Cycle Assessment (LCA) of Hybrid Photovoltaic/Thermal (PV/T) solar systems for domestic applications, Renewable Energy 126 (2018) 708-723.

[13] L. Brottier, R. Bennacer, Thermal performance analysis of 28 PVT solar domestic hot water installations in Western Europe, Renewable Energy 160 (2020) 196-210.

[14] C. Kutlu, M.T. Erdinc, J. Li, Y. Wang, Y. Su, A study on heat storage sizing and flow control for a domestic scale solar-powered organic Rankine cycle-vapour compression refrigeration system, Renewable Energy 143 (2019) 301-312.

[15] A. Arabkoohsar, G.B. Andresen, A smart combination of a solar assisted absorption chiller and a power productive gas expansion unit for cogeneration of power and cooling, Renewable Energy 115 (2018) 489-500.

[16] H. Chen, Z. Li, Y. Xu, Evaluation and comparison of solar trigeneration systems based on photovoltaic thermal collectors for subtropical climates, Energy Conversion and Management 199 (2019) 111959.

[17] D. Gong, R. Niu, Y. Xu, J. Min, H. Liu, X. Cheng, B. Yang, C. Ke, X. Wang, Q. Li, K. Li, Z. Cui, Thermal shocking resistance of AlCrNO-based solar selective absorbing coating prepared by cathodic arc plating, Solar Energy 180 (2019) 8-15.

[18] K. Valleti, S.G. Rao, P. Miryalkar, A. Sandeep, D.S. Rao, Cr-(CrN/TiAlN)m-AlSiN-AlSiO open-air stable solar selective coating for concentrated solar thermal power applications, Solar Energy Materials and Solar Cells 215 (2020) 110634.

[19] M. Lämmle, A. Oliva, M. Hermann, K. Kramer, W. Kramer, PVT collector technologies in solar thermal systems: A systematic assessment of electrical and thermal yields with the novel characteristic temperature approach, Solar Energy 155 (2017) 867-879.

[20] L. Evangelisti, R. De Lieto Vollaro, F. Asdrubali, Latest advances on solar thermal collectors: A comprehensive review, Renewable and Sustainable Energy Reviews 114 (2019) 109318.

[21] G. Sadeghi, M. Najafzadeh, M. Ameri, Thermal characteristics of evacuated tube solar collectors with coil inside: An experimental study and evolutionary algorithms, Renewable Energy 151 (2020) 575-588.

[22] Q. Wang, M. Hu, H. Yang, J. Cao, J. Li, Y. Su, G. Pei, Performance evaluation and analyses of novel parabolic trough evacuated collector tubes with spectrum-selective glass envelope, Renewable Energy 138 (2019) 793-804.

[23] M.B. Elsheniti, A. Kotb, O. Elsamni, Thermal performance of a heat-pipe evacuated-tube solar collector at high inlet temperatures, Applied Thermal Engineering 154 (2019) 315-325.

[24] P. Henshall, P. Eames, F. Arya, T. Hyde, R. Moss, S. Shire, Constant temperature induced stresses in evacuated enclosures for high performance flat plate solar thermal collectors, Solar Energy 127 (2016) 250-261.

[25] F. Arya, R. Moss, T. Hyde, S. Shire, P. Henshall, P. Eames, Vacuum enclosures for solar thermal panels Part 1: Fabrication and hot-box testing, Solar Energy 174 (2018) 1212-1223.

[26] F. Arya, R. Moss, T. Hyde, S. Shire, P. Henshall, P. Eames, Vacuum enclosures for solar thermal panels Part 2: Transient testing with an uncooled absorber plate, Solar Energy 174 (2018) 1224-1236.

[27] R. Moss, S. Shire, P. Henshall, F. Arya, P. Eames, T. Hyde, Performance of evacuated flat plate solar thermal collectors, Thermal Science and Engineering Progress 8 (2018) 296-306.

[28] R.W. Moss, P. Henshall, F. Arya, G.S.F. Shire, P.C. Eames, T. Hyde, Simulator testing of evacuated flat plate solar collectors for industrial heat and building integration, Solar Energy 164 (2018) 109-118.

[29] R.W. Moss, P. Henshall, F. Arya, G.S.F. Shire, T. Hyde, P.C. Eames, Performance and operational effectiveness of evacuated flat plate solar collectors compared with conventional thermal, PVT and PV panels, Applied Energy 216 (2018) 588-601.

[30] R.W. Moss, G.S.F. Shire, P. Henshall, P.C. Eames, F. Arya, T. Hyde, Design and fabrication of a hydroformed absorber for an evacuated flat plate solar collector, Applied Thermal Engineering 138 (2018) 456-464.

[31] D. Gao, G. Gao, J. Cao, S. Zhong, X. Ren, Y.N. Dabwan, M. Hu, D. Jiao, T.H. Kwan, G. Pei, Experimental and numerical

analysis of an efficiently optimized evacuated flat plate solar collector under medium temperature, Applied Energy 269 (2020) 115129.

[32] L. Jiang, C. Lan, Y.S. Kim, Y. Ma, R. Winston, An evacuated PV/Thermal hybrid collector with the tube/XCPC design, World Renewable Energy Forum, WREF 2012, Including World Renewable Energy Congress XII and Colorado Renewable Energy Society (CRES) Annual Conference, 2012, pp. 88-94.

[33] A.Y.A. Oyieke, F.L. Inambao, Performance Characterisation of a Hybrid Flat-Plate Vacuum Insulated Photovoltaic/Thermal Solar Power Module in Subtropical Climate, International Journal of Photoenergy 2016 (2016) 1-15.

[34] C. Kutlu, J. Li, Y. Su, Y. Wang, G. Pei, S. Riffat, Investigation of an innovative PV/T-ORC system using amorphous silicon cells and evacuated flat plate solar collectors, Energy 203 (2020).

[35] J. Ji, C. Guo, W. Sun, W. He, Y. Wang, G. Li, Experimental investigation of tri-functional photovoltaic/thermal solar collector, Energy Conversion and Management 88 (2014) 650-656.

[36] C. Guo, J. Ji, W. Sun, J. Ma, W. He, Y. Wang, Numerical simulation and experimental validation of tri-functional photovoltaic/thermal solar collector, Energy 87 (2015) 470-480.

[37] M. Hu, B. Zhao, X. Ao, Suhendri, J. Cao, Q. Wang, S. Riffat, Y. Su, G. Pei, An analytical study of the nocturnal radiative cooling potential of typical photovoltaic/thermal module, Applied Energy 277 (2020) 115625.

[38] M. Hu, B. Zhao, X. Ao, X. Ren, J. Cao, Q. Wang, Y. Su, G. Pei, Performance assessment of a trifunctional system integrating solar PV, solar thermal, and radiative sky cooling, Applied Energy 260 (2020) 114167.

[39] J. Zhou, X. Ma, X. Zhao, Y. Yuan, M. Yu, J. Li, Numerical simulation and experimental validation of a micro-channel PV/T modules based direct-expansion solar heat pump system, Renewable Energy 145 (2020) 1992-2004.

[40] S.-Y. Wu, T. Wang, L. Xiao, Z.-G. Shen, Effect of cooling channel position on heat transfer characteristics and thermoelectric performance of air-cooled PV/T system, Solar Energy 180 (2019) 489-500.

[41] A. Jha, P. Tripathy, Heat transfer modeling and performance evaluation of photovoltaic system in different seasonal and climatic conditions, Renewable energy 135 (2019) 856-865.

[42] X. Huang, W. Li, H. Fu, D. Li, C. Zhang, H. Chen, Y. Fang, K. Fu, S.P. DenBaars, S. Nakamura, S.M. Goodnick, C.-Z. Ning, S. Fan, Y. Zhao, High-Temperature Polarization-Free III-Nitride Solar Cells with Self-Cooling Effects, ACS Photonics 6(8) (2019) 2096-2103.

[43] R. Vaillon, O. Dupre, R.B. Cal, M. Calaf, Pathways for mitigating thermal losses in solar photovoltaics, Scientific Reports 8(1) (2018) 13163.

[44] X. Ren, J. Li, M. Hu, G. Pei, D. Jiao, X. Zhao, J. Ji, Feasibility of an innovative amorphous silicon photovoltaic/thermal system for medium temperature applications, Applied Energy 252 (2019) 113427.